Deep-seated gravitational slope deformation scaling on Mars and Earth: same fate for different initial conditions and structural evolutions

Olga Kromuszczyńska[1], Daniel Mège[2,3,4], Krzysztof Dębniak[1], Joanna Gurgurewicz[1,2], Magdalena Makowska[1] and Antoine Lucas[5]

[1]Institute of Geological Sciences, Polish Academy of Sciences, Research Centre in Wrocław, Podwale 75, 50-449 Wrocław, Poland
[2]Space Research Centre, Polish Academy of Sciences, Bartycka 18A, 00-716 Warsaw, Poland
[3]Laboratoire de Planétologie et Géodynamique, Université de Nantes, UMR CNRS 6112, 2 rue de la houssinière, Nantes, France
[4]Observatoire des Sciences de l'Univers Nantes Atlantique, OSUNA CNRS UMS 3281, Nantes, France
[5]Institut de Physique du Globe de Paris, Sorbonne Paris Cité, Université Paris, Diderot, Paris 75013, France

Correspondence to: Daniel Mège (dmege@cbk.waw.pl)

Abstract. Some of the most spectacular instances of deep-seated gravitational slope deformation (DSGSD) are found on Mars in the Valles Marineris region. They provide an excellent opportunity to study DSGSD phenomenology using a scaling approach. The topography of selected DSGSD scarps in Valles Marineris and in the Tatra Mountains is investigated after their likely similar postglacial origin is established. The deformed Martian ridges are larger than the deformed terrestrial ridges by one to two orders, with however a similar height-to-width ratio, ~0.24. The measured finite strain of the Valles Marineris ridges is 3 times larger than in the Tatra Mountains, suggesting that starting from two different initial conditions, with steeper slopes in Valles Marineris, the final ridge geometry is now similar. Because DSGSD is expected to be now inactive in both regions, their comparison suggests that whatever the initial ridge morphology, DSGSD proceeds until a mature profile is attained. On both planets, strain is distributed over the same number (~5) of major scarps; fault displacements are therefore much larger on Mars. The large offsets make necessary reactivation of the DSGSD fault scarps in Valles Marineris, whereas single seismic events would be enough to generate DSGSD fault scarps in the Tatra Mountains. The required longer activity of the Martian faults may be correlated with a long succession of climate cycles generated by the unstable Mars obliquity. In spite of similar global geometry today, the studied ridges on Mars and Earth affected by DSGSD did not start from similar initial conditions and did not follow the same structural evolution.

1 Introduction

1.1 The dissected Valles Marineris hillslopes

The Valles Marineris bedrock hillslopes show a dissected, "spur-and-gully" morphology at a glance similar to the morphology of alpine mountains, locally degraded at the first order into tributary canyons and huge landslides (Lucchitta, 1978; Patton,

5   1991; Lucchitta et al., 1992). Spur-and-gully dissection has taken the form of subparallel, digitate spurs separated by gullies covered by long slope deposits (Lucchitta, 1978; Howard, 1989). The upper parts of the slopes are steeper than the lower parts (Lucchitta, 1978). The latter are covered by talus of material accumulated at the angle-of-repose (Patton, 1981). The spurs are usually perpendicular to the slope; however, in some areas, their oblique orientation relative to chasma trend suggests structural control by vertical fractures oblique to the troughs that must be tens of kilometres long (Sharp 1973; Blasius et al., 1977).

10   High resolution image data available since the early 2000's have revealed that outside these tributary canyons and huge landslides, the dissected, pristine morphology shows a variety of smaller-scale geomorphological features which are familiar to mountain geomorphologists, with the association or superimposition of a rich variety of landforms controlled by mountain permafrost degradation, streams erosion, talus development, and gravity (Mège and Bourgeois, 2011; Gourronc et al., 2014; Dębniak et al., 2017). The difference with alpine mountain geomorphology on Earth is therefore not that much a matter of

15   morphological details; it rather lies in the size of the landsystems. In the main troughs, the height of the Valles Marineris slopes is several kilometres, and up to 10 km, whereas typical mountain slopes on Earth are hundreds to a few kilometres high.

1.2 Deep-seated gravitational slope deformation in Valles Marineris

This work focuses on a series of morphotectonic features observed along Valles Marineris walls displaying the spur-and-gully morphology, including uphill-facing normal faults scarps and crestal grabens. Such features are systematically observed when

20   spur-and-gully dissection occurs on internal ridges within the main Valles Marineris chasmata. They denote extensional tectonics, but boundary forces that result in crustal "rifting" are unlikely to be the cause of this deformation even though rifting is frequently considered to have been a major contributor to the formation of some of the main Valles Marineris chasmata (e.g., Masson, 1977; Frey, 1979; Schultz, 1991, 1995a, 1998; Mège and Masson, 1996a, 1996b; Peulvast et al., 2001; Mège et al., 2017). One of the main reasons is that uphill-facing scarps and crestal grabens have not been reported to have formed in

25   terrestrial rift zones on Earth nor are they expected to form in experimental models (e.g., Corti, 2012 for the East African Rift System). In extreme cases, when crustal stretching has been on the order of hundreds of percent, cracking and normal faulting is pervasive in horsts as much as in grabens (Angelier and Colletta; 1983), which has certainly not been the case in Valles Marineris (e.g. Schultz 1991, 1995a; Mège and Masson 1996b; Mège et al. 2003).

Another reason is that when the basal ridge slope topography can be accurately studied (i.e. not mantled by debris aprons),

30   normal faulting on the ridge crest and slopes appears to be counterbalanced by basal slope bulging (Mège and Bourgeois, 2011). Ridge-top splitting has been interpreted by Lucchitta et al. (1992) and Treiman (2008) as crustal zones strengthened by dyke intrusion or cemented by central fractures. Arguing that such a fracture origin is not well documented on Earth either,

Mège and Bourgeois (2011), Kromuszczyńska et al. (2012) and Gourronc et al. (2014) interpreted these features as an effect of deep-seated gravitational slope deformation (DSGSD). Uphill-facing normal faulting and crestal extensional deformation is indeed well documented on Earth in areas of DSGSD (review in Mège and Bourgeois, 2011). In most described terrestrial instances, such as in the Alps of Europe, Japan and New Zealand, the Andes and others, where DSGSD has been described in

5 mountain ridges glaciated during the Quaternary (review in Mège and Bourgeois, 2011), Such a postglacial context, in the Valles Marineris case, is adapted to the recently identified and widespread glacial landsystem (Gourronc et al., 2014; Mège et al., 2017; Dębniak et al., 2017), is also in agreement with expected slope deformation in this context (Makowska et al., 2016), and additionally provides a good framework to understand the detected mineralogical occurrences as from CRISM (Mège and Bourgeois, 2011; Cull et al., 2014). Postglacial deformation, as far as DSGSD is concerned, includes the paraglacial response

10 of rock slopes to changing stress conditions after glacier retreat, (e.g., Ballantyne, 2002), i.e. hillslope debuttressing, but also some longer term deformation made possible or facilitated by slope debuttressing. This includes upslope migration of stress release, and postglacial water flow, pressure variations and subcritical failure occurring for instance within the framework of the geologic response to climate cyclicity (Pánek et al., 2017).

In this work, we will therefore assume that DSGSD is the most likely origin for the uphill-facing scarps and crestal grabens

15 observed on the slopes of the Valles Marineris spur-and-gully ridges. We also consider that a postglacial origin is likely, given its consistency and adaptation to the evidence of a widespread Valles Marineris glacial landsystem subject to short-period climatic variations (Laskar et al., 2004; Levrard et al., 2004) under which additional slope morphologies may develop (e.g., Quantin et al. 2005; Chojnacki et al., 2016).

1.3 Scaling of processes involved in deep-seated gravitational slope deformation

20 Some gravity processes do not similarly develop at different scales. For instance, landslide propagation does not depend on fully similar parameters when small and large. Landslides that are small with respect to mountain size are influenced by the surrounding mountainous topography, the first effect of which being the development of an inclined transport channel that overlies an accumulation of debris on a less inclined slope. An example is the Thurwieser landslide in the central Alps (e.g., Sosio et al., 2008). For landslides that involve a large fraction of the mountain slope, the deposits spread in the nearly flat

25 valley or plain downstream, such as in the case of the Socompa rock avalanche (e.g., Kelfoun and Druitt, 2005). Although similar at first order, landslide propagation is not controlled by the same parameters because the landslide slope is different. Farin et al. (2014) and Borykov et al. (submitted) showed that landslide volume controls landslide propagation when the slope angle of the propagation plane is steeper than ca. 20°, whereas it has no influence for more gentle slopes.

This dependency of landslide propagation on slope, and indirectly on volume (and friction), initially identified on laboratory

30 experiments (Farin et al., 2014), could be adequately documented by natural examples thanks to some very large Martian landslides (Borykov et al., submitted), much larger than any terrestrial landslide, which help populate the landslide dataset for voluminous landslides that propagate on nearly flat surfaces. Similar to landslides, DSGSD occurs on mountain slopes that are much smaller on Earth than on Mars, and at the first order, their origin may be similar. However, like in the case of landslides,

the difference in scale may be associated with differences in controlling parameters. We will not answer this complex question in this work, but instead provide quantitative information that may help in future works aiming at constraining the parameters that control DSGSD over a broad range of sizes.

1.4 Scaling with the Tatra Mountains

5   We compare DSGSD in Valles Marineris with DSGSD in the Tatra Mountains in Slovakia and Poland (Fig. 1), a historic region of DSGSD investigations (Jahn, 1964; Nemčok, 1972; Mahr, 1977). Investigating this potential analogue area is motivated both by some similarity in DSGSD development conditions, and easy field access.

DSGSD develops independent of the structure and lithology of the topographic ridge, although major strength contrasts affect the strain field and therefore the expected observed deformation (e.g., Makowska et al., 2016). Such contrasts may be provided

10   by weak/strong rock contrasts and major faults. In Valles Marineris, the upper part of the slopes are thought to be volcanic, akin to trap series (McEwen et al., 1999. Beyer and McEwen, 2005), with thin lava layering in which jointing is pervasive. This level may be viewed as a typical homogeneous rock mass (Hoek, 1983; Schultz, 1995b). The ridge material that makes the lower part of the ridges are usually covered by debris slopes. Nevertheless, when they are observed they appear to be made of a massive basement rock or magmatic intrusives (Williams et al., 2003). DSGSD scarps were studied in the Tatra Mountains

15   during two periods of field work. The measured scarps are located in a granodioritic intrusive body (Nemčok et al., 1994). In both Valles Marineris and the studied sites of the Tatra Mountains, the role of the tectonic fabric in the development of the DSGSD features is therefore expected to be minor, although elsewhere in the Tatra Mountains a tectonic breccia level parallel to DSGSD displacement has been suspected to have influenced scarp development (Pánek et al., 2017).

In the Tatra Mountains, deglaciation was ended at ~8500 B.P. (Lindner et al., 2003), and the ages obtained for DSGSD in the

20   Polish and Slovakian Tatras are between 15.7-4.3 ka (Pánek et al., 2017). Some DSGSD features in the Tatra Mountains started soon after local deglaciation, but the influence of climatic cycles and their geological consequences, especially in terms of groundwater flow, pore pressure variations, and their implications for rock corrosion, is suspected to be major because in some instances scarp development sometimes occurred well after deglaciation. In Valles Marineris, the glacial landsystem cannot be dated with a similar accuracy, and observations (Mège and Bourgeois, 2011) are not against several or many periods of

25   glaciations since the upper Hesperian. Martian climate instability actually favours the interpretation of many glaciation and deglaciation cycles, a response to incessant planetary obliquity variations (Laskar et al., 2004). For instance, climate oscillations were shown to proceed with a rate as fast as 120,000 year per cycle in the last 10 million years (Levrard et al., 2004). Development of DSGSD features in Valles Marineris is therefore likely to have proceeded in response to a variety of processes recurrently operating over a very long history; both short-term processes such as ridge postglacial debuttressing, and

30   long-term evolution under the influence of liquid water in a melting mountain permafrost (e.g. Noetzli and Gruber, 2009; Huggel et al., 2013).

DSGSD in Valles Marineris and the Tatra Mountains are probably not active anymore, therefore while comparing both regions, we are comparing finite deformation in ridges assumed to be akin to homogeneous rock masses at the first order.
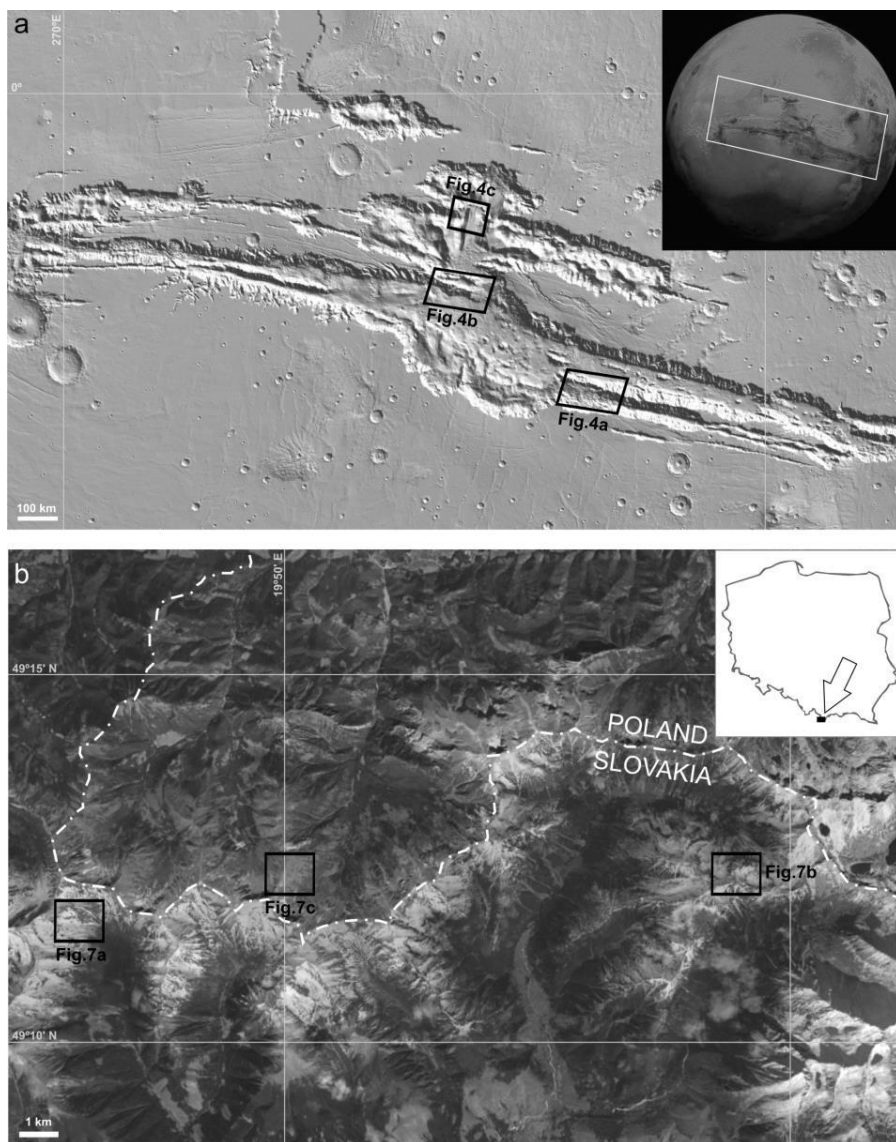
Figure 1: Location of the study sites: a. Valles Marineris; MOLA-based shaded relief map b. Tatra Mts.; Google™ Earth; 2016 CNES/Astrium.

2 Data and methods

2.1 Data

The observations of the Valles Marineris trough system reported here were done using Mars Reconnaissance Orbiter/CTX imagery as a baseline (Fig. 2). Higher resolution images from Mars Reconnaissance Orbiter HiRISE were used for more detailed research when available. For topography, the resolultion of the HRSC digital elevation model (DEM) mosaic of Valles

Marineris (Gwinner et al., 2009) is too coarse for this work, whereas HiRISE DEMs would be adapted but were either not available in the study sites, or did not cover enough surface to be used. DEMs generated from CTX stereo pairs have the appropriate vertical precision of ca. 10 m, and were used to extract topographic profiles. Nevertheless, some DSGSD sites (including e.g. in Ius Chasma) could not be investigated due to the poor geometry of the CTX images available during the lifetime of this project, which did not make possible generation of good quality DEMs.

Elevation data in the Tatra Mountains were collected using the GPS device Garmin GPSMap 62s in differential and non-differential mode, as explained in Kromuszczyńska et al. (2016), during two field campaigns conducted in September 2012 and June 2013 in the Higher Tatra Mountains in Poland and Slovakia, and the Lower Tatra Mountains in Slovakia.

CTX
Resolution: 6 m/pxl
Swath width: 30 km

HiRISE
Resolution: 0,25 m/pxl
Swath width: 6 km

CTX DEM
Grid spacing: 30 m
Vertical accuracy: 15 m
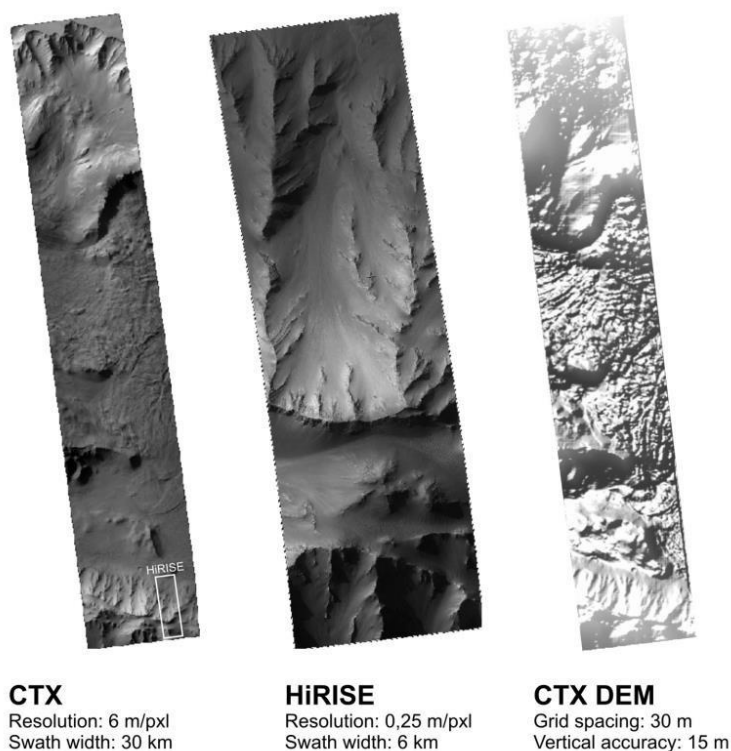
Figure 2: Types of data used in the Martian part of this study, here at the Coprates Chasma site.

2.2 Methods

The deformation produced by DSGSD on Mars and Earth are compared by quantitative interpretation of topographic profiles. Profile generation and analysis is done with ArcGIS 3D Analyst. The topographic profiles are then analysed in a graphic software.

On the basis of the DEMs (in case of Martian study sites) and field observations (in case of terrestrial study sites), as well as the profiles themselves, the mean local ridge slopes are identified and marked. Then, the faults cutting the profiles are located

and marked as two lines illustrating two mean fault dip angles, α=60º and α=70º (Fig. 3), representative of unrotated shallow normal faults in extensional settings on Earth (e.g., Gudmundsson, 1992; Acocella et al., 2003). The trace of DSGSD scarps in map view both in Valles Marineris and in the Tatras sites, indicate that vertical fractures play a negligible role in ridge deformation.

5   Fault mechanics equations do not scale with gravity, implying that similar angles are expected on Martian rocks than in terrestrial rocks. The 10º angle interval is considered as the error on the true angular value, which cannot be retrieved from topography due to fault scarp erosion and debris accumulation. The vertical and horizontal displacements on DSGSD fault scarps are measured as on Fig.3.
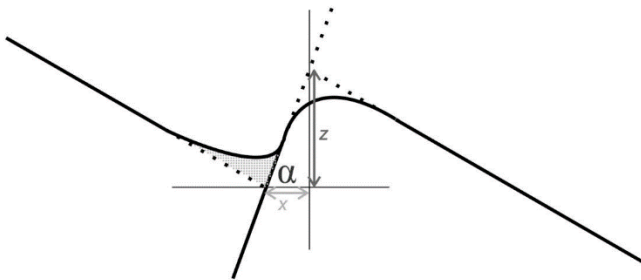
10   **Figure 3: Parameters used for calculation of vertical and horizontal displacement across uphill-facing normal fault scarp; α is fault dip angle, x is horizontal fault displacement, and z is vertical fault displacement.**

The measured fault displacements are scaled in a second step. This allows to compare the scarps between the 6 study sites. The scaled horizontal displacement is calculated by dividing the average value $\bar{x}$ of horizontal fault displacement x measured on the ridge by the width L of the ridge:

15    $$Dh = \bar{x}/L \tag{1}$$

The scaled vertical displacement Dv is obtained by dividing the average value $\bar{z}$ of vertical fault displacement z measured on the ridge by the height of the ridge H:

$$Dv = \bar{z}/H \tag{2}$$

The ratio R of ridge height H to width L, or aspect ratio, of the studied ridges allows to examine the similarity in the shape of 20   the ridges as observed today, after DSGSD:

$$R = H/L \tag{3}$$

In order to compare the finite deformation of ridges, the maximum displacement found on each site is used, and is inferred from the maximum displacement measured along each profile:

$$\Delta x = \max\left(\sum_{i=1}^{n1} x_{p1}^i, \dots, \sum_{i=1}^{nN} x_{pN}^i\right) \tag{4}$$

25   and

$$\Delta z = \max\left(\sum_{i=1}^{n1} z_{p1}^i, \dots, \sum_{i=1}^{nN} z_{pN}^i\right) \tag{5}$$

where Δx is horizontal strain and Δz is vertical strain for each site, respectively, containing n scarps along a given $p1, ..., pN$ profile. In the case of Δz, the profiles from a single ridge slope are taken into account in order to avoid vertical displacement duplication.

In terms of strain, the maximum strain found on each site is:

$$\varepsilon_x = \Delta x / L \tag{6}$$

and

$$\varepsilon_z = -\Delta z / H \tag{7}$$

3 Study sites

Three sites with clearly visible DSGSD features were selected in Valles Marineris, based on DEM generation possibility, and three in the Tatra Mountains (Table 1).

Site ID	Site	Coordinates (central point)	H (m)	L (m)	R
1	Coprates Montes	67º54'W; 12º18'S	5 500	22 000	0.25
2 (a)	Melas-Candor ridge	73º55'W; 8º00'S	5 000	56 000	0.08
2 (b)	Melas-Candor ridge	73º55'W; 8º00'S	5 000	30 000	0.25
3	Candor-Ophir ridge	73º25'W; 4º56'S	5 700	35 000	0.18
4	Jamnícke sedlo	19º46'06''E; 49º12'02''N	250	900	0.28
5	Veľká Garajova kopa	19º58'37''E; 49º12'05''N	200	750	0.27
6	Ornak	19º50'11''E; 49º12'33''N	420	2 200	0.19

Table 1: Ridge location and parameters in the three Valles Marineris sites and the three Tatra sites. The reason for distinguishing between 2(a) and 2(b) is given in the Section 4.

3.1 Valles Marineris

Study Site 1 is located in the westernmost part of Coprates Montes, in Coprates Chasma (Fig. 4a). DSGSD there takes a form of crestal graben, and uphill-facing normal faults scarps on the northern side of the ridge. The western and eastern parts of the first study site are separated by a 26 km wide landslide alcove, with a scar aligned on both sides with the scarps of DSGSD crestal graben. Site 2 is the ridge separating Melas and Candor chasmata (Fig. 4b). Eastward, the ridge splits at the middle and lowers eastward almost down to the chasma floor, interpreted as a consequence of increased crestal extension by Mège and

Bourgeois (2011), then reinterpreted as a glacial valley developed along a former crestal graben by Gourronc et al. (2014). Uphill-facing normal fault scarps developed on both ridge sides. Site 3 is a ridge located between Candor and Ophir chasmata (Fig. 4c). DSGSD features are represented by distinct crestal graben, which cause the ridge-top to split. On the slopes uphill-facing normal fault scarps are slightly visible. The global ridge parameters are given in Table 1.
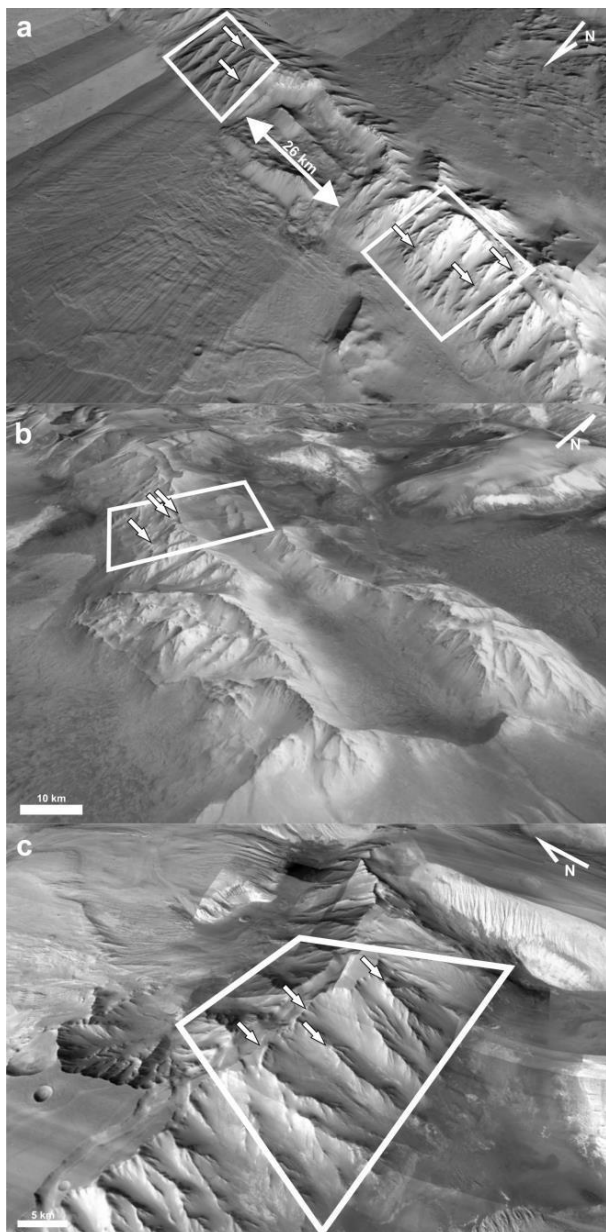
Fig. 4. Martian study sites: a. Site 1: Coprates Montes. DSGSD is observed on the ridge on both sides of the landslide; b. Site 2: Melas-Candor boundary ridge; c. Site 3: Candor-Ophir boundary ridge. The boxes locates the areas where the profiles were measured (Fig. 6). Arrows indicate the DSGSD scarps. MRO/CTX mosaic draped on Mars Express/HRSC topography.

3.2 Tatra Mountains

Sites 4 and 5 are located in the Slovakian Tatra Mountains, and Site 6 in the Polish Tatras. Site 4 (Fig. 5a) contains DSGSD features on a ridge east of Jamnícke Sedlo and Ostrý Roháč summit. A few uphill-facing normal faults scarps cut the ridge on its both slopes. The crest is wide and clearly reworked by DSGSD activity. The height of individual scarps reaches up to 5-10

5 m. Site 5 (Fig. 5b) is a ridge west of Veľká Garajova Kopa on the way to Veľká Kopa. In the west, DSGSD features express as uphill-facing normal fault scarps distributed over the whole slope and associated with soil creep. In the east, the crest becomes narrower, uphill-facing normal fault scarps are restricted to close to the crest, and ridge-top splitting occurs by way of fresh, 20-cm wide tension fractures. The 900 m wide ridge rises up to 250 m above the adjacent valleys. The height to width ratio R is 0.28. In this area, a few uphill-facing normal faults scarps cut the ridge on its both slopes. The crest is wide and

10 clearly reworked by DSGSD activity. The height of the scarps reaches 5-10 m. Site 6 (Fig. 5c) includes DSGSD features on the ridge south of the Ornak summit. The ridge has a wide crest cut with a series of normal faults on both sides that generated high uphill-facing scarps. The height of the highest scarps exceeds 10 m.
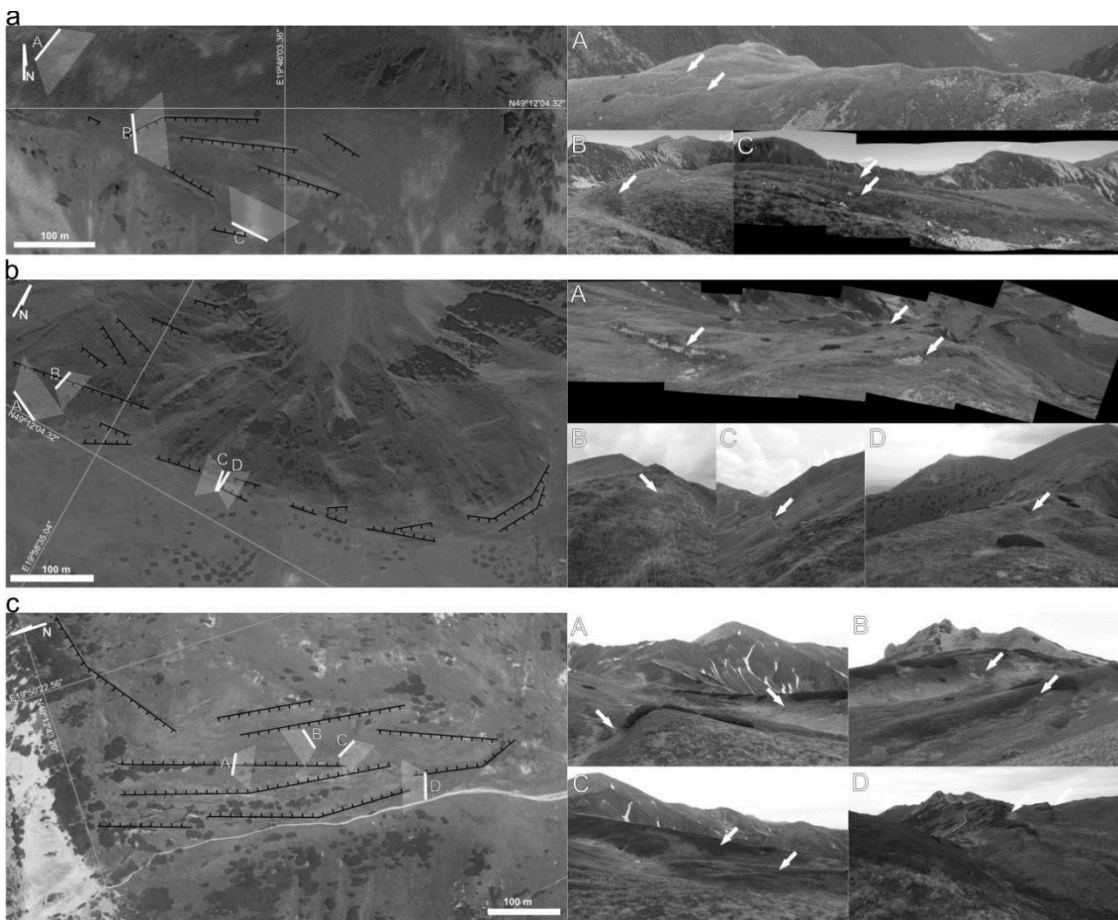
Figure 5: Terrestrial study sites: a. Site 4, east from Jamnícke Sedlo; b. Site 5: a ridge west of Veľká Garajova Kopa; c. Site 6: ridge
15 **south from Ornak. Arrows indicate the DSGSD scarps. Google™ Earth; 2015 CNES/Astrium.**

4 Results

4.1 Fault displacement observed along topographic profiles

On Mars, 11 topographic profiles were measured in Site 1 (Fig. 6a). In sites 2 and 3, 5 and 6 profiles were obtained, respectively (Fig. 6b-c). On Earth, 9 profiles were obtained in Site 4 and 13 in sites 5 and 6 (Fig. 7a-c). Profiling perpendicular to the ridges

5   was conducted along crest lines, resulting in broken profile traces, and along straight lines. In a given site, these two methods yielded similar results. As examples, profiles following spur-and gully crest lines are provided for the Martian sites 1 and 3. All the fault displacement measurements are provided as Supplementary Material.
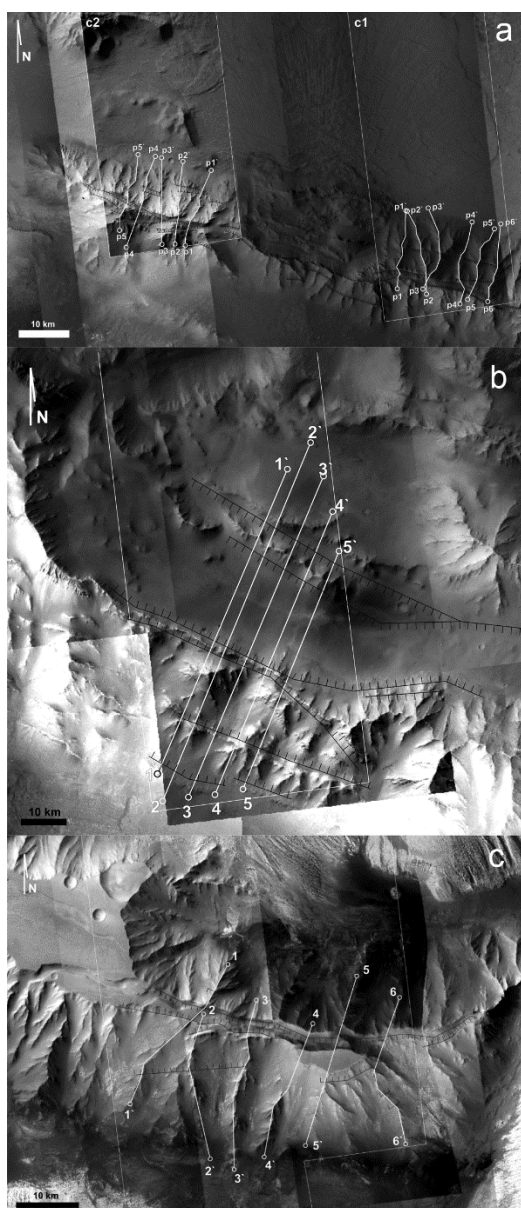
Figure 6: Martian sites, location of the analysed fault scarps (black), CTX DEM (white boxes) and profiles (numbered white lines) used for fault displacement analysis. (a) Site 1; (b) Site 2; (c) Site 3. MRO/CTX mosaic.
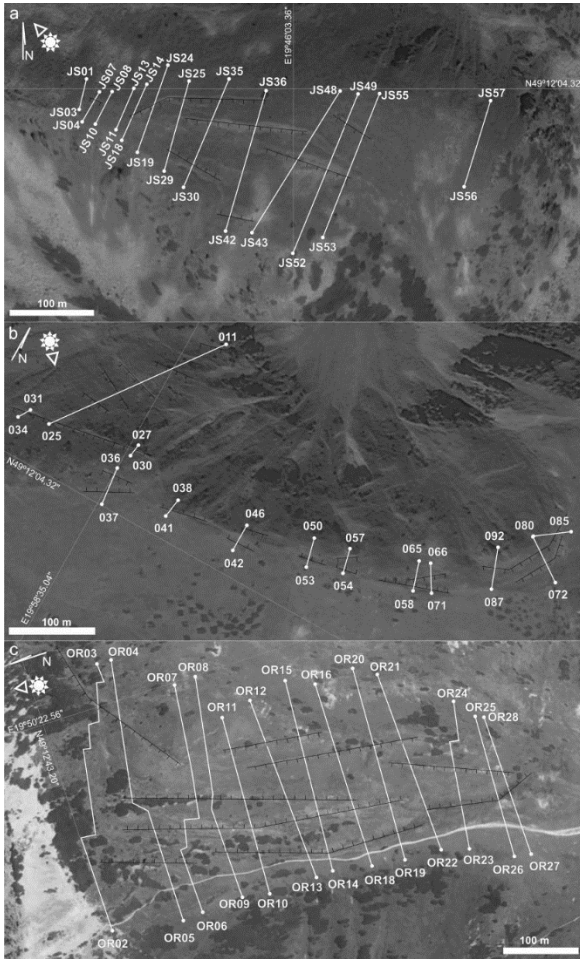
Fig. 7. Terrestrial sites, location of the profiles. (a) Site 4, across a crest line east from Jamnícke Sedlo; (b) Site 5, the ridge west from Veľká Garajova Kopa; (c) Site 6, a ridge south from Ornak. Google™ Earth; 2015 CNES/Astrium.

Two interpretations have been done of the central valley of Site 2, which have implications for DSGSD measurement. If it is a central graben similar to the central graben in e.g. Site 1 that underwent further extension, as interpreted by Mège and Bourgeois (2011), the valley depth is a proxy to the crestal graben height. Alternatively, if it is a glacial valley (Gourronc et al., 2014), then there is no crestal graben observed. In that case, it is likely that a crestal graben of unknown depth existed, and guided the orientation of the glacial valley before being fully ablated. For this reason, profiles for Site 2 consider two options: one with 6 normal fault scarps (consistent with Mège and Bourgeois, 2011), and one with the 3 southernmost and the northernmost scarps only (consistent with Gourronc et al., 2014). Both options represent end-members in which DSGSD in the site is maximised and minimised.

In the Tatra Mountains, the profiles were recorded along straight profiles, except in a few cases where vegetation made necessary deflection of the walking path, with a measured vertical precision of 40 cm (Kromuszczyńska et al., 2016). Examples of interpreted profiles are given on Fig. 8. In sites 1 and 3, the largest displacements are found to have occurred along crestal graben faults.
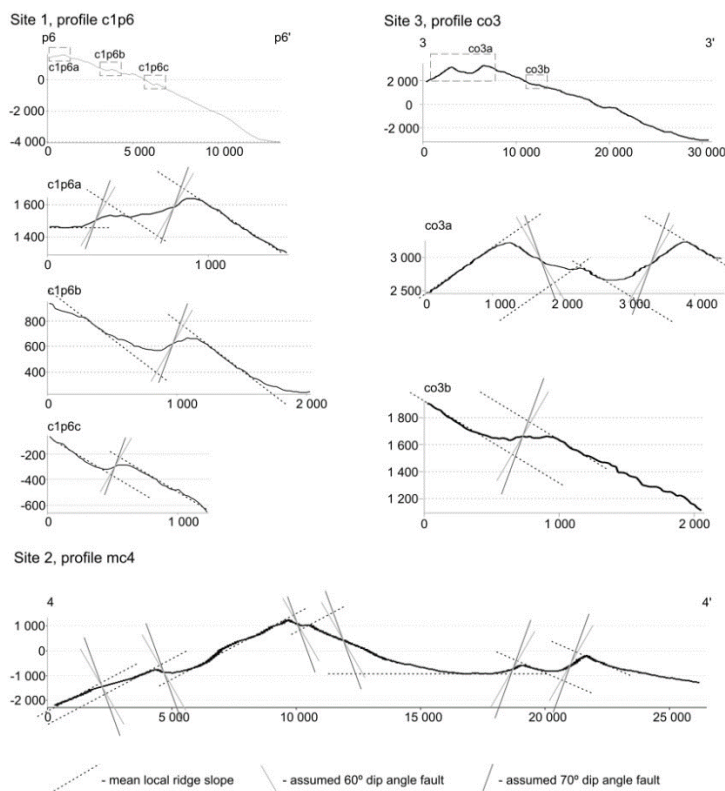
Figure 8a: Reconstructed fault traces (continuous lines) measured in the three Martian study sites, assuming fault dips of 60° and 70°. The values on both axes are given in meters.
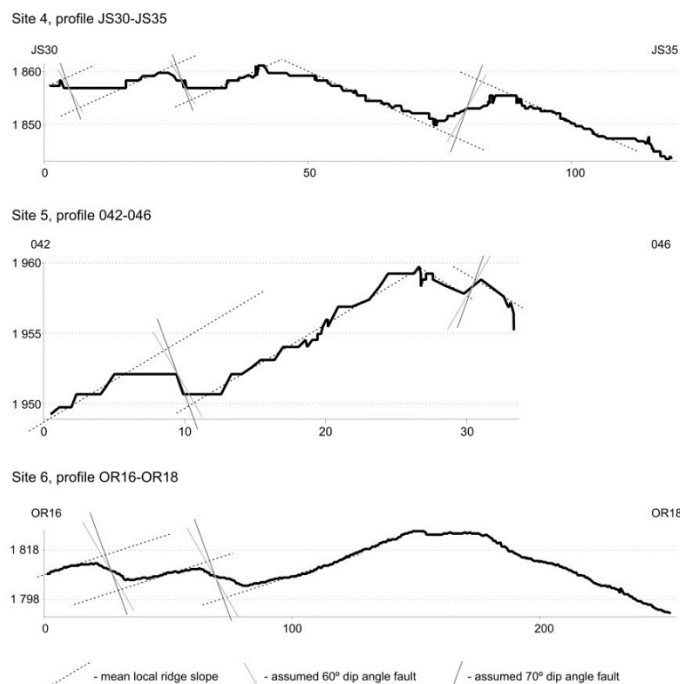
Fig. 8b. Representative fault displacements measured in the three Tatra study sites, assuming fault dips of 60° and 70°. The values on both axes are given in meters.

The mean measured displacements are reported in Table 2.

Site ID	Mean horizontal fault displacement (m)		Mean vertical fault displacement (m)	
α	60°	70°	60°	70°
1	174	115	307	323
2(a)	569	383	952	1022
2(b)	421	289	726	794
3	312	214	538	584
4	4.5	3.1	7.9	8.5
5	2.3	1.6	3.9	4.3
6	6.5	4.4	10.3	11.1

Table 2. Mean horizontal and vertical displacements at the six study sites. 2(a) assumes that the central valley in Site 2 is of purely DSGSD origin, whereas 2(b) assumes that the central valley has a purely glacial origin.

4.2 Fault displacement scaling with ridge dimensions

The scaled displacements are presented on Fig. 9. Although displacement along the fault scarps are two orders higher on Mars than on Earth (Table 2), once scaled to ridge dimensions (eqs. 1 and 2), this difference becomes much less prominent (Fig. 9a-b). *Dh* for the Valles Marineris sites (~0.006) is roughly three times the values for the Tatras sites (~0.002) only. Similar

5   difference occurs in *Dv* (~0.07 vs. ~0.02).
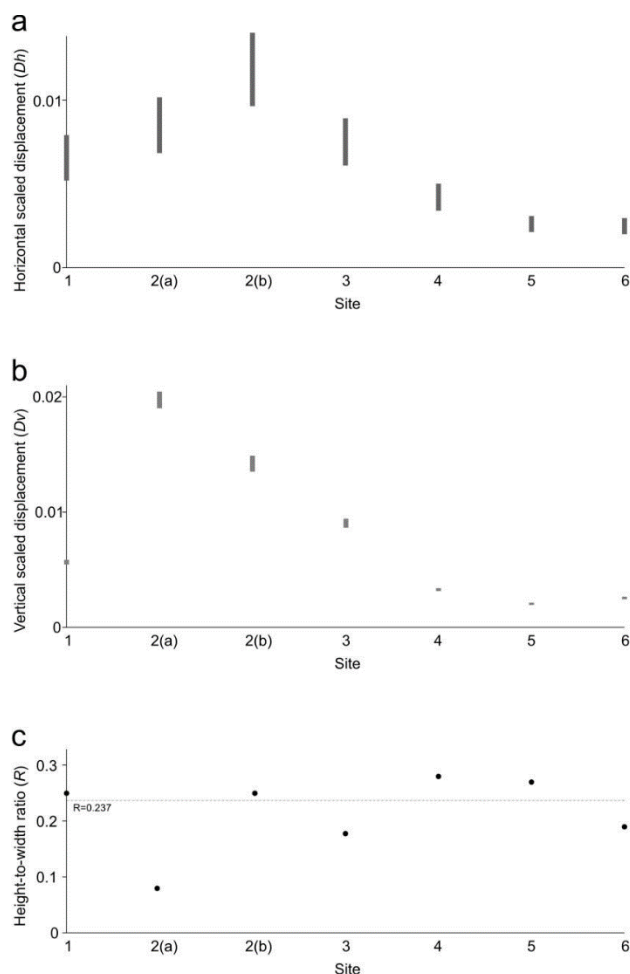
Figure 9: Scaled horizontal displacement *Dh* (a) scaled vertical displacement *Dv* (b), and height to width ratios *R* (c) in the study sites. For Site 2, two end-members fault displacement interpretations of the Melas Chasma - Candor Chasma intervening depression

10   **are given: option (a) corresponds to the fully tectonic interpretation proposed by Mège and Bourgeois (2011) and option (b) to a mixed tectonic/glacial interpretation (Gourronc et al., 2014). Dashed line in 9c indicates the average height-to-width ratio when the option (b) of site 2 is considered.**

In Site 2, *Dv* is much higher than in the other Valles Marineris sites, whatever the interpretation of the morphology (Fig. 9b, Site 2a or 2b). This is interpreted as a consequence of removal of the highest part of the ridge, as discussed in Section 5. *Dv* is therefore overestimated by an unknown amount.

Why is DSGSD fault displacement on Mars of the same order as on Earth once scaled? The smaller gravity acceleration at the
5   surface of Mars (3.71 m·s^{-2}) than at the surface of Earth (9.81 m·s^{-2}) tends to increase the stability of Martian topographic ridges compared to terrestrial ridges having similar height and slope angles (Makowska et al., 2016). Conversely, the much more voluminous ridges on Mars tend to build a higher gravitational potential, and make Martian ridges more deformable. These results show that both effects tend to compensate.

Discussion

10   **5.1 Fault strain distribution**

It is remarkable that in spite of much larger cumulated fault displacements (Fig. 8), the number of DSGSD faults in Valles Marineris (Tables 2 to 4) is not significantly different from the number of such faults in the Tatra Mountains.

The very large fault offsets measured on individual faults in Valles Marineris require cumulated events (e.g., Fossen, 2010). The gradual dominance of slip along master faults with deformation time in a given fault set, at the expense of small faults, is
15   a consequence of fault linkage with growing deformation (Cartwright et al., 1995). Because DSGSD is observed at surface and does not extend much deep below the base level of the deforming ridge (e.g., Makowska et al., 2016), the normal stress is small, which makes stable sliding more likely than stick-slip sliding (Marone and Scholz, 1988). Larger fault slip in Valles Marineris is therefore made possible by plastic ridge deformation over a time span longer than the deformation time of the Tatra Mountains ridges. The valley glaciers expected to have occupied Valles Marineris chasmata floors are larger than the
20   valley glaciers in the Tatra Mountains by at least two orders (Mège and Bourgeois, 2011; Gourronc et al., 2014), ridge slope deglaciation may have taken a long time, promoting long-lasting fault slip during DSGSD. Furthermore, the chaotic orbital obliquity regime of Mars (Laskar et al. 2004) makes realistic a very large number of glaciation and deglaciation cycles in Valles Marineris throughout the history of Mars, and as many glacier advance and retreat cycles generating incremental DSGSD-induced fault displacements. In contrast, the paraglacial structures in the Tatra Mountains are not expected to be older
25   than 400 ka (Lindner et al., 2003). Clay gouge infilling (Treiman, 2008) of possible pre-existing fractures along the ridges inherited from the formation of Valles Marineris (Schultz, 1995a; Mège and Masson, 1996a, 1996b) may have also promoted stable sliding (Fossen, 2010) under the new glacial loading conditions.

5.2 DSGSD dependency on ridge scale

The ridge aspect ratio *R* (eq. 3) informs on whether DSGSD, which is thought to have stopped on all the ridges, attained a
30   similar final stage. The range of *R* is narrow (0.18 – 0.29) for Earth and Mars if the glacial valley at Site 2 is fully erosional (Fig. 9c, Site 2b), as interpreted by Gourronc et al. (2014). *R* values are much more scattered (0.08 – 0.29) and atypical

compared with the two other Martian sites if the central valley in Site 2 is of DSGSD origin only (Fig. 9c, Site 2a). Because of data coherence, we find the interpretation that the glacial valley is of fully erosional origin more likely.

An implication of the similar aspect ratio of all the profiles is that DSGSD has evolved from initial geometries that may have been different but eventually converged toward a common final and stable shape, in which the ridge aspect ratio is ~0.24.

5   DSGSD therefore tends to stop to a stabilised state that is not scale dependent.

5.3 Initial ridge geometries

Analysis of the cumulated fault displacements (Table 3) can be used to retrieve information on the initial ridge geometries. The total horizontal extension (eq. 4) and vertical contraction (eq. 5) in the Tatras ridges is of the order of tens of meters, corresponding to total horizontal elongation (eq. 6) and vertical shortening (eq. 7) of 0.8 – 1.2% horizontally and 8.6 – 16%

10   vertically. In Valles Marineris, deformation is two orders larger, with total horizontal elongation 2 – 7% and vertical shortening of 21 – 52%. The proportionally larger deformation in Valles Marineris than in the Tatras, in spite of similar ridge aspect ratio, suggests that DSGSD evolved to its finite stage from an initially different aspect ratio.

Site ID	Δx [m]		Δz [m]		εx		εz	
	60°	70°	60°	70°	60°	70°	60°	70°
1	1250	840	1740	1790	0.06	0.04	-0.32	-0.33
2(a)	3670	2480	3980	4240	0.07	0.04	-0.80	-0.85
2(b)	1370	940	2350	2580	0.05	0.03	-0.47	-0.52
3	1250	840	1220	1350	0.04	0.02	-0.21	-0.24
4	16.4	10.9	28.2	29.9	0.02	0.01	-0.11	-0.12
5	15.6	11.5	27.2	31.4	0.02	0.02	-0.14	-0.16
6	26	18	36	38	0.012	0.008	-0.086	-0.090

Table 3: Ridge deformation in response to DSGSD in Valles Marineris and the Tatra Mountains. Δx: cumulated horizontal ridge elongation; Δz: cumulated vertical shortening; ε_x: horizontal strain (horizontal displacement normalized to ridge width in Table 1);
15 **ε_z: vertical strain (vertical displacement normalized to ridge height), respectively. Elongation is positive and shortening is negative. 2(a) assumes that the central valley in Site 2 is of purely DSGSD origin, whereas 2(b) assumes that the central valley has a purely glacial origin. Hypothesis (b) is considered to be more likely (see the Discussion).**

Conclusion

The ridges displaying DSGSD features in Valles Marineris are larger than the ridges displaying DSGSD in the Tatra Mountains
20   by one order. In both regions, DSGSD is thought to have come to an end. Their aspect ratio (height/width) is similar, ~0.24 (Table 1). However, finite strain of the Valles Marineris ridges is three times higher than the finite strain of the Tatras ridges,

implying that the initial slopes of the Valles Marineris ridges were higher than those of the Tatras ridges. It may be inferred that on the one hand, the maturity or immaturity (instability) of ridges affected by DSGSD may be inferred from their aspect ratio. On the other hand, this final, stabilised ridge geometry does not carry indication on the initial shape of the ridge itself, an information that may be retrieved only by collecting information from individual DSGSD scarp.

5   Individual fault displacements across DSGSD scarps in the Tatra Mountains are similar to fault displacement in most DSGSD sites on Earth (see references in the Supplementary Table 1 of Mège and Bourgeois, 2011), which suggests that this conclusion may be extrapolated to other regions. Nevertheless, similar analyses need to be conducted in other ridges affected by DSGSD, both inactive and active, before general conclusions can be drawn.

DSGSD in the Tatra Mountains and Valles Marineris sites studied here occurred in rocks that at the first order may be
10 considered as initially mechanically homogeneous. Rheological contrasts such as provided by lithologic contrasts or tectonic fabric may however be critical parameters in the control of the geometry of a ridge subject to DSGSD (e.g., Makowska et al., 2016), and its evolution. The conclusions drawn here will probably be modified if the ridge structure departs too much from the homogeneous rock mass assumed here.

Basal ridge deformation in response to gravitational spreading of the upper part of the ridge was not explicitly considered in
15 this work. Its characterisation is usually complicated by the incision and accumulation processes that commonly affect basal slopes. Basal deformation is however implicitly included in the ridge aspect ratio.

Fault displacement homothety implies that fault growth in both regions may not have been similar. Fault growth in the Tatras is consistent with single seismic events (yet to be formally identified in the field) for each scarp, whereas many events are required to explain the large offsets measured across the Valles Marineris DSGSD fault scarps. Fault reactivation may have
20 occurred as a geologic response to the long succession of glacial/interglacial cycles expected to have occurred throughout the history of Valles Marineris (Laskar et al., 2004). In summary, although currently of globally similar geometry, the ridges affected by DSGSD in Valles Marineris and in the selected sites of the Tatra Mountains did not have the same initial conditions, nor is their structural evolution similar.

Acknowledgements

25   This work is financially supported by the Foundation for Polish Science, project FNP TEAM/2011-7/9 "Mars: another planet to approach geoscience issues" and the OPUS/V-MACS project no. 2015/17/B/ST10/03426 of the National Science Centre, Poland.

References

Acocella, V., Behncke, B., Neri, M., and D'Amico, S.: Link between major flank slip and 2002–2003 eruption at Mt. Etna
30   (Italy), Geophys. Res. Lett., 30(24), 2286, doi:10.1029/ 2003GL018642, 2003.

Angelier, J. and Colletta, B.: Tension fractures and extensional tectonics., Nature, 301, 4951, 1983.

Ballantyne, C. K.: Paraglacial geomorphology, Quaternary Science Reviews 21, 19352017, doi: 10.1016/S0277-3791(02)00005-7, 2002.

Beyer, R. A. and McEwen, A. S.: Layering stratigraphy of eastern Coprates and northern Capri Chasmata, Mars. Icarus, 179, 1-23, 2005.

Blasius, K. R., Cutts, J. A., Guest, J. E. and Masursky, H.,: Geology of the Valles Marineris: First Analysis of Imaging From the Viking 1 Orbiter Primary Mission, J. Geophys. Res., 82(28), 4067, 1977.

Borykov, T., Mège, D., Mangeney, A., Richard, P., Gurgurewicz, J., and Lucas, A., Investigation of frictional weakening of Martian and terrestrial landslides using discrete element simulations, submitted to Landslides, March 6, 2018.

Cartwright, J. A., Trudgill, B. D., and Mansfield, C.: Fault growth by segment linkage: An explanation for scatter in maximum displacement and trace length data from the Canyonlands Grabens of SE Utah, J. Struct. Geol., 17, 1319–1326, 1995.

Chojnacki, M., McEwen, A. S., Dundas, C., Ojha, L., Urso, A., and Suton, S., Geologic context of recurring slope lineae in Melas and Coprates Chasmata, Mars, J. Geophys. Res.: Planets, doi:10.1002/2015JE004991, 2016.

Corti, G.: Evolution and characteristics of continental rifting: Analog modeling-inspired view and comparison with examples from the East African Rift System, Tectonophysics, 522–523,1–33, 2012.

Cull, S., McGuire, P., Gross, C., Myers, J., and Shmorhun, N.: A new type of jaroite deposit on Mars: Evidence for past glaciation in Valles Marineris? Geology, 42(11), 959-962, 2014.

Dębniak, K., Mège, D., and Gurgurewicz, J., Geomlorphology of Ius Chgasma, Valles Marineris, Mars, J. Maps, 13(2), 260-269, 2017

Farin, M., Mangeney, A., and Roche, O.: Fundamental changes of granular flow dynamics, deposition, and erosion processes at high slope angles: Insights from laboratory experiments, J. Geophys. Res.: Earth Surface, 10.1002/2013JF002750, 2014.

Fossen, H.: Structural geology, Cambridge Univ. Press, 463 p., 2010.

Frey, H.: Martian canyons and African rifts: structural comparisons and implications. Icarus, 37, 142-155, 1979.

Gourronc, M., Bourgeois, O., Mège, D., Pochat, S., Bultel, B., Massé, M., Le Deit, L., Le Mouélic, S., and Mercier, D.: One million cubic kilometers of fossil ice in Valles

Marineris: relics of a 3.5 Gy old glacial landsystem along the Martian equator, Geomorphology, 204, 235-255, doi: 10.1016/j.geomorph.2013.08.009, 2014.

Gudmundsson, A.: Formation and growth of normal faults at the divergent plate boundary in Iceland, Terra Nova, 4, 464–471, doi: 10.1111/j.1365-3121.1992.tb00582.x, 1992.

Gwinner, K., Scholten, F., Spiegel, M., Schmidt, R., Giese, B., Oberst, J., Heipke, C., Jaumann, R., and Neukum, G.: Derivation and validation of high-resolution digital terrain models from Mars Express HRSC data, Photogramm. Eng. Remote Sens., 75, 1127-1142, 2009.

Hoek, E.: Strength of jointed rock masses, Géotechnique, 23, 187-223, 1983.

Howard, A. D.: Miniature analog of spur-and-gully landforms in Valles Marineris, Rep. Planetary Geology and Geophysics Program, NASA TM 4130, 355-357, 1989.

Huggel, C., Salzmann, N., and Allen, S.: High-mountain slope failures and recent and future warn extreme events, In: Climate Forcing of Geological Hazards, McGuire, B., and Maslin, M. (eds.), John Wiley & Sons, 195-222, 2013.

Jahn, A.: Slope morphological features resulting from gravitation, Z. Geomorph., Supplt 5, 59–72, 1964.

Kelfoun, K. and Druitt, T. H.: Numerical modelling of the emplacement of Socompa rock avalanche, Chile, J. Geophys. Res., 110, B12202, doi:10.1029/2005JB003758, 2005.

Kromuszczyńska, O., Mège, D., Lucas, A., Gurgurewicz, J.: Giant sackung in Valles Marineris. 43rd Lunar Planet. Sci. Conf., Houston, TX, Abstract 1161, 2012.

Kromuszczyńska, O., Mège, D., Castaldo, L., Gurgurewicz, J., Makowska, M., Dębniak, K. and Jelínek, R.: Evaluation of the EGNOS service for topographic profiling in field geomorphology, Geomorphology, 268, 253-265, doi: 10.1016/j.geomorph.2016.05.026, 2016.

Laskar, J., Correia, A. C. M., Gastineau, M., Joutel, F., Levrard, B. and Robutel, P.: Long term evolution and chaotic diffusion of the insolation quantities of Mars, Icarus 170(2), 343364, doi: 10.1016/j.icarus.2004.04.005, 2004.

Levrard, B., Forget, F., Mountmessin, F., and Laskar, J.: Recent ice-rich deposits formed at high latitudes on Mars by sublimation of unstable equatorial ice during low obliquity, Nature, 431, 1072-1075, 2004.

Lindner, L., Dzierżek, J., Marciniak, B., and Nitychoruk, J.: Outline of Quaternary glaciations in the Tatra Mts: their development, age and limits, Geol. Quart., 47, 269-280, 2003.

Lucchitta, B. K.: Morphology of chasma walls, Mars, J. Res. U.S. Geological Survey, 6, 5, 651-662, 1978.

Lucchitta, B. K., McEwen, A. S., Clow, G. D., Geissler, P. E., Singer, R. B., Schultz, R. A. and Squyres, S. W.: The canyon system on Mars, In: Mars, Kieffer, H. H., Jakosky, B. M., Snyder, C. W. and Matthews, M. S. (eds.), 453-492, University of Arizona Press, Tucson, 1992.

Mahr, T.: Deep-reaching gravitational deformations of high mountain slopes, Bull. Int. Assoc. Eng. Geol., 16, 121–127, 1977.

Makowska, M., Mège, D., Gueydan, F. and Chéry, J.: Mechanical conditions and modes of paraglacial deep-seated gravitational spreading in Valles Marineris, Mars, Geomorphology, 268, 246-252, doi: 10.1016/j.geomorph.2016.06.011, 2016.

Marone, C. and Scholz, C. H.: The depth of seismic faulting and the upper transition from stable to unstable slip regimes, Geophys. Res. Lett., 15, 621-624, 1988.

Masson, P.: Structure pattern analysis of the Noctis Labyrinthus-Valles Marineris regions of Mars, Icarus, 30, 49-62, 1977.

McEwen, A. S., Malin, M. C., Carr, M. H., and Hartmann, W. K.: Voluminous volcanism on early Mars revealed in Valles Marineris, Nature, 397, 584-586, 1999.

Mège, D. and Bourgeois, O.: Equatorial glaciations on Mars revealed by gravitational collapse of Valles Marineris wallslopes, Earth Planet. Sci. Lett., 310, 182-191, doi: 10.1016/j.epsl.2011.08.030, 2011.

Mège, D. and Masson, P.: A plume tectonics model for the Tharsis province, Mars, Planet. Space Sci., 44, 1499–1546, 1996a.

Mège, D. and Masson, P.: Amounts of stretching in Valles Marineris, Mars, Planet. Space Sci., 44, 8, 749-782, 1996b.

Mège, D., Cook, A. C., Lagabrielle, Y., Garel, E., and Cormier, M.-H.: Volcanic rifting at Martian grabens, J. Geophys. Res.: Planets, 108 (E5), 5044, doi:10.1029/2002JE001852, 2003.

5   Mège, D., Le Deit, L., Rango, T., and Korme, T.: Gravity tectonics of topographic ridges: halokinesis and gravitational spreading in the western Ogaden, Ethiopia, Geomorphology, 193, 113, doi:10.1016/j.geomorph.2013.03.018, 2013.

Mège, D., Bourgeois, O., and Gurgurewicz, J.: Origin of the northern Valles Marineris trough: tectonics and subglacial erosion, Lunar Planet. Sci. Conf., Abs. 1110, 2017.

Nemčok, A.: Gravitational slope deformation in high mountains. Proc. 24th Int. Geol. Congr., 13, 132–141, 1972.

10   Nemčok, J., Bezák, V., Biely, A., Gorek, A., Gross, P., Halouzka, R., Janák, M., Kahan, Š., Kotański, Z., Lefeld, J., Mello J., Reichwalder, P., Raczkowski, W., Roniewicz, P., Ryka, W., Wieczorek, J., Zelman J.: Geological map of the Tatra Mountains, MŽP SR, GÚDŠ, Bratislava, 1994.

Noetzli, J. and Gruber, S.: Transient thermal effects in Alpine permafrost, Cryosph., 3, 85-99, 2009.

Pánek, T., Mentlik, P., Engel, Z., Braucher, R., Zondervan, A., and Aster Team: Late Quaternary sackungen in the highest

15   mountains of the Carpathians, Quat. Sci. Rev., 159, 47-62, 2017.

Patton, P. C.: Evolution of the spur and gully topography on the Valles Marineris wall scarps, NASA Tech. Memo. 84211, 324-325, 1981.

Peulvast, J.-P., Mège, D., Chiciak, J., Costard, F., and Masson, P. L.: Morphology, evolution and tectonics of Valles Marineris wallslopes (Mars), Geomorphology, 37, 329–352, 2001.

20   Quantin, C., Allemand, P., Mangold, N., Dromard, G., and Delacourt, C.: Fluvial and lacustrine activity on layered deposits in Melas Chasma, Valles Marineris, Mars, J. Geophys. Res.: Planets, 110, E12S19, doi:10.1029/2005JE002440, 2005.

Schultz, R. A.: Structural development of Coprates Chasma and Western Ophir Planum, Valles Marineris Rift, Mars. J. Geophys. Res., 96 (E5), 22777-22792, doi: 10.1029/91JE02556, 1991.

Schultz, R. A.: Gradients in extension and strain at Valles Marineris, Mars, Planet. Space Sci., 43, 1561–1566, 1995a.

25   Schultz, R. A.: Limits on strength and deformation properties of jointed basaltic rock masses, Rock Mech. Rock Eng., 28(1), 1-15, 1995b.

Schultz, R. A.: Multiple-process origin of Valles Marineris basins and trough, Mars, Planet. Space Sci., 46(6/7), 827-834, 1998.

Sharp, R. P.: Mars: Troughed terrain, J. Geophys. Res., 78 (20), 4063-4072, 1973.

30   Sosio, R., Crosta, G. B., and Hungr, O.: Complete dynamic modeling calibration for the Thurwieser rock avalanche (Italian Central Alps), Eng. Geol., 100, 11-26, 2008.

Treiman A. H., Fault-trace ridges, Valles Marineris, Mars: Evidence for large-scale fault controlled paleo-groundwater flow, Nature Geosci., 1, doi:10.1038/ngeo131, 2008.

Williams, J. P., Paige, D. A., and Manning, C. E., Layering in the wall rock of Valles Marineris: intrujsive and extrusive magmatism. Geophys. Res. Lett., 30(12), 1623, doi:10.1029/2003GL017662, 2003.